

RESEARCH ARTICLE

10.1002/2015JD023603

Key Points:

- GCMs partition condensate phase dependent upon temperature
- 20–80% of GCM LWP response to warming is due to the repartitioning of condensate
- Model spread in LWP response is reduced using a single glaciation temperature

Supporting Information:

- Figure S1

Correspondence to:

D. T. McCoy,
dtmccoy@atmos.uw.edu

Citation:

McCoy, D. T., D. L. Hartmann, M. D. Zelinka, P. Ceppi, and D. P. Grosvenor (2015), Mixed-phase cloud physics and Southern Ocean cloud feedback in climate models, *J. Geophys. Res. Atmos.*, *120*, 9539–9554, doi:10.1002/2015JD023603.

Received 29 APR 2015

Accepted 19 AUG 2015

Accepted article online 21 AUG 2015

Published online 25 SEP 2015

Mixed-phase cloud physics and Southern Ocean cloud feedback in climate models

Daniel T. McCoy¹, Dennis L. Hartmann¹, Mark D. Zelinka², Paulo Ceppi^{1,3}, and Daniel P. Grosvenor⁴

¹Atmospheric Sciences, University of Washington, Seattle, Washington, USA, ²Program for Climate Model Diagnosis and Intercomparison, Lawrence Livermore National Laboratory, Livermore, California, USA, ³Department of Meteorology, University of Reading, Reading, UK, ⁴School of Earth and Environment, University of Leeds, Leeds, UK

Abstract Increasing optical depth poleward of 45° is a robust response to warming in global climate models. Much of this cloud optical depth increase has been hypothesized to be due to transitions from ice-dominated to liquid-dominated mixed-phase cloud. In this study, the importance of liquid-ice partitioning for the optical depth feedback is quantified for 19 Coupled Model Intercomparison Project Phase 5 models. All models show a monotonic partitioning of ice and liquid as a function of temperature, but the temperature at which ice and liquid are equally mixed (the glaciation temperature) varies by as much as 40 K across models. Models that have a higher glaciation temperature are found to have a smaller climatological liquid water path (LWP) and condensed water path and experience a larger increase in LWP as the climate warms. The ice-liquid partitioning curve of each model may be used to calculate the response of LWP to warming. It is found that the repartitioning between ice and liquid in a warming climate contributes at least 20% to 80% of the increase in LWP as the climate warms, depending on model. Intermodel differences in the climatological partitioning between ice and liquid are estimated to contribute at least 20% to the intermodel spread in the high-latitude LWP response in the mixed-phase region poleward of 45°S. It is hypothesized that a more thorough evaluation and constraint of global climate model mixed-phase cloud parameterizations and validation of the total condensate and ice-liquid apportionment against observations will yield a substantial reduction in model uncertainty in the high-latitude cloud response to warming.

1. Introduction

The response of Southern Ocean (SO) low clouds to warming remains a significant source of uncertainty in global warming simulations. The uncertainties in the low cloud response are primarily due to lack of agreement as to how cloud albedo changes [Zelinka *et al.*, 2012a, 2012b, 2013]. This is consistent with the substantial low cloud cover in the SO region [McCoy *et al.*, 2014b], and the role of low cloud feedback as the largest source of disagreement between GCMs [Bony *et al.*, 2006; Vial *et al.*, 2013]. The Southern high latitudes, and to a lesser degree, the Northern high latitudes show a pronounced increase in upwelling shortwave radiation in a warmed climate (a negative feedback) that transitions to a slight decrease in upwelling shortwave radiation in the subtropics (a positive feedback) [Zelinka *et al.*, 2012a, 2013]. This dipole in SW feedback poses an interesting problem as it is highly robust across different global climate models (GCMs), but its exact placement and magnitude vary significantly between GCMs. The response of SO albedo to warming affects both the local radiative feedback and the atmospheric circulation [Ceppi *et al.*, 2014; Frierson and Hwang, 2012].

Previous observational and modeling studies have indicated that the increase in cloud albedo at high latitudes is likely to be significantly influenced by transitions from ice to liquid as relatively less reflective ice transitions to bright liquid droplets [Cheng *et al.*, 2012; McCoy *et al.*, 2014a; Naud *et al.*, 2006; Tsushima *et al.*, 2006; Zelinka *et al.*, 2012a]. The glaciation process in nature is complicated and poorly constrained [Atkinson *et al.*, 2013; Murray *et al.*, 2012], and the physics and dynamics of mixed-phase clouds are nonlinear [Morrison *et al.*, 2011]. The transition from liquid to ice is subject both to the availability of ice nuclei and to the complex microphysical interactions of supercooled liquid and ice nuclei.

Based on our understanding of the mechanisms that drive mixed-phase cloud, it is likely that declining ice condensate fractions would lead to an increase in liquid condensate that is larger than the reduction in ice condensate, so that the total mass of condensate should increase as the cloud deglaciates [Klein *et al.*, 2009; McCoy *et al.*, 2014a; Morrison *et al.*, 2011]. Several mechanisms are thought to contribute to this effect:

(1) precipitation is suppressed as ice becomes less dominant; (2) cloud top radiative cooling is enhanced as liquid becomes more dominant, which in turn enhances in-cloud turbulence; (3) surface longwave radiative heating and atmospheric cooling is enhanced as liquid becomes more dominant, decreasing static stability and enhancing surface moisture and energy fluxes [Morrison *et al.*, 2011; Tsushima *et al.*, 2006]. Other mechanisms, such as the enhancement of liquid water content with the change in the temperature derivative of the moist adiabat as the climate warms [Betts and Harshvardhan, 1987], should further enhance the liquid water path (LWP) beyond the transitions engendered by the repartitioning of condensate. While these processes do not include all possible mechanisms that may be at play in mixed phase cloud, they provide a working hypothesis rooted in observations that would lead to an increase in condensate mass as clouds move to a more deglaciated state.

In this study we analyze Coupled Model Intercomparison Project Phase 5 (CMIP5) simulations to estimate the relative roles of condensate mass increases and phase changes in explaining the response of LWP to warming over the Southern Ocean. First, in section 3, we study the relationship between temperature and the fraction of condensate that is liquid in the models. We then estimate the relative contributions of the changes in liquid fraction and total condensed water mass to the shortwave feedbacks in the models in section 4. Finally, in section 6, we estimate the contribution of the variations of the temperature dependence of the liquid fraction to the spread in the LWP response to warming among the models.

2. Data

Monthly mean model data are collected from 19 CMIP5 GCMs. This study uses two monthly climatologies to compare the warmed and historical climates. The historical climatology is created using output from the historical simulations from the period 1850–1900, and the warmed climatology is created using output from the Representative Concentration Pathways 8.5 (RCP8.5) simulations from 2050 to 2100. The grid box mean cloud mass fraction of ice (archived as *cli*) and liquid (*clw*) are used for each model and experiment. These variables are archived on the CMIP5 cloud vertical grid. Atmospheric temperature is interpolated to the cloud grid. The mass of ice and liquid in each vertical grid box of a model are calculated using the *cli* and *clw* variables. The integrated mass of ice and liquid in a given pressure level are referred to in this study as $IWP(p)$ and $LWP(p)$. The vertically integrated cloud fraction and precipitation are also retrieved for each model where available. Throughout the remainder of this study data may be assumed to be on the cloud vertical grid, and unless stated otherwise, on the native latitude-longitude grid of each model.

3. Diagnosis of GCM Mixed-Phase Behavior

Given the poor constraints on ice nucleation, GCMs may either parameterize the transition from liquid to ice as a simple function of temperature [Bower *et al.*, 1996; Cesana *et al.*, 2015; Choi *et al.*, 2014] or attempt a more rigorous approach including nucleation and growth [Cesana *et al.*, 2015; Komurcu *et al.*, 2014]. Careful study and intercomparison of ice nucleation parameterizations between GCMs have shown that nucleation and processes subsequent to nucleation contribute equally to the uncertainty in mixed-phase behavior of several GCMs with advanced microphysics parameterizations [Komurcu *et al.*, 2014]. Although ice microphysics are complex, one would expect to find that warmer temperatures on average lead to higher abundances of liquid and lower abundances of ice, provided that the concentration of IN does not vary significantly with temperature [Bower *et al.*, 1996; Hu *et al.*, 2010; Kanitz *et al.*, 2011; Tan *et al.*, 2014].

Data from historical runs spanning 1850–1900 are used to determine the way that each model partitions condensate. The data are subset into the latitude region 30°S–80°S. All longitudes, months, and pressure levels are included. Liquid condensate fraction (LCF) is defined as liquid mass over the sum of ice and liquid mass. We use the term condensate to indicate the sum of liquid and ice cloud mass. The LCF is calculated from *cli* and *clw* and is composited on temperature. The compositing procedure does not make any differentiation by pressure, latitude, longitude, or month of the year. In nature, the freezing of cloud droplets is governed by several factors: temperature, ice nuclei concentration, and cloud condensation nuclei concentration. Because we are interested in the response to warming of mixed-phase clouds, we want to extract an effective temperature dependence from the models and composite the LCF on temperature alone. Observational studies have shown that LCF is strongly dependent on temperature

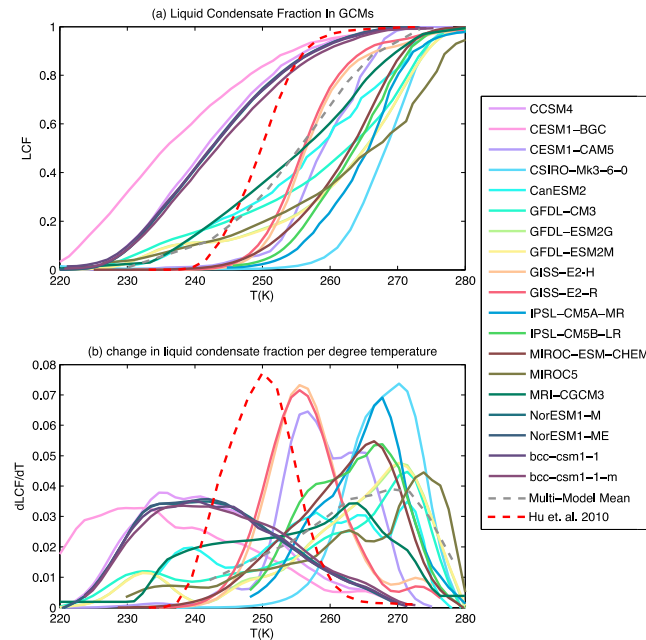


Figure 1. (a) The diagnosed mixed-phase partitioning from the historical experiment for the years 1850–1900 in the 30°S–80°S latitude band. Observations from Hu et al. [2010] are shown as a dashed red line. The multimodel mean is shown as a dashed grey line. (b) The slope of the LCF curve at each temperature.

[Bower et al., 1996; Hu et al., 2010; Kanitz et al., 2011]. LCF is shown as a function of temperature for each model in Figure 1a. Some GCMs have more variability in LCF within a given temperature bin, but LCF has a clear monotonic dependence on temperature in all models (Figure S1 in the supporting information). The rate of change in LCF is also shown as a function of temperature (Figure 1b) to indicate the temperature range in which LCF is most sensitive to temperature in each model. It should be noted that due to the monthly time resolution of the data available for the CMIP5 models, the mean temperature and LCF are used to represent the effective dependence of LCF on temperature. It is likely that GCMs that do not utilize a temperature ramp have a larger variance about mean LCF (Figure S1). Using monthly data does not hamper our analysis because we are interested in the mean change in cloud properties with warming.

Examination of the LCF as a function of temperature across GCMs shows a wide variety of partitioning behaviors. The temperature at which ice and liquid are equally abundant (which we refer to as the glaciation temperature) varies by almost 40 K between models in Figure 1. Previous studies have warned that the parameterization of glaciation may introduce bias in the cloud feedback in GCMs, so that this wide range of glaciation temperatures is especially interesting [Naud et al., 2006]. In addition, the sensitivity of the optical depth feedback to the repartitioning of ice and liquid in a warming climate is expected to be especially large due to the combination of high cloud fraction and small cloud droplet effective radius in this region [McCoy et al., 2014b].

The mechanisms that drive ice nucleation in the remote marine boundary layer are poorly understood, but empirical fits to global remote sensing observations from the Cloud-Aerosol Lidar and Infrared Pathfinder Satellite Observation (CALIPSO) instrument allow us to compare a global observational estimate of the temperature dependence of LCF to the model behavior in Figure 1 [Hu et al., 2010, 2009]. The observed dependence of cloud top LCF on temperature is also shown in Figure 1. This observational estimate falls in the middle of the range of GCM behaviors. It should be noted that this might not be an entirely appropriate comparison because the CALIPSO instrument measures the phase near cloud top, since lidar is rapidly attenuated in cloud, while the GCM LCF is averaged over each vertical grid box. Unfortunately, other remotely sensed estimates of cloud phase capable of significant cloud penetration must still rely on a parameterized thermodynamic phase [Huang et al., 2012; Naud et al., 2010].

It is unclear whether the use of cloud top LCF would lead to a lower or higher LCF than if the LCF measured throughout the vertical extent of the cloud were to be used. A thin layer of liquid water at cloud top overlaying an ice layer [Rauber and Tokay, 1991] would tend to push the LCF measured by CALIPSO toward being too high relative to the true LCF of the cloud as a whole. In situ measurements of Southern Ocean clouds conducted in Grosvenor et al. [2012] mostly showed very low ice concentrations in Southern Ocean clouds in agreement with the High-performance Instrumented Airborne Platform for Environmental Research Pole-to-Pole Observations global transects found no significant below cloud top prevalence of ice particles, suggesting it is unlikely that a large underlying ice layer exists that cannot be detected by CALIPSO [Chubb et al., 2013].

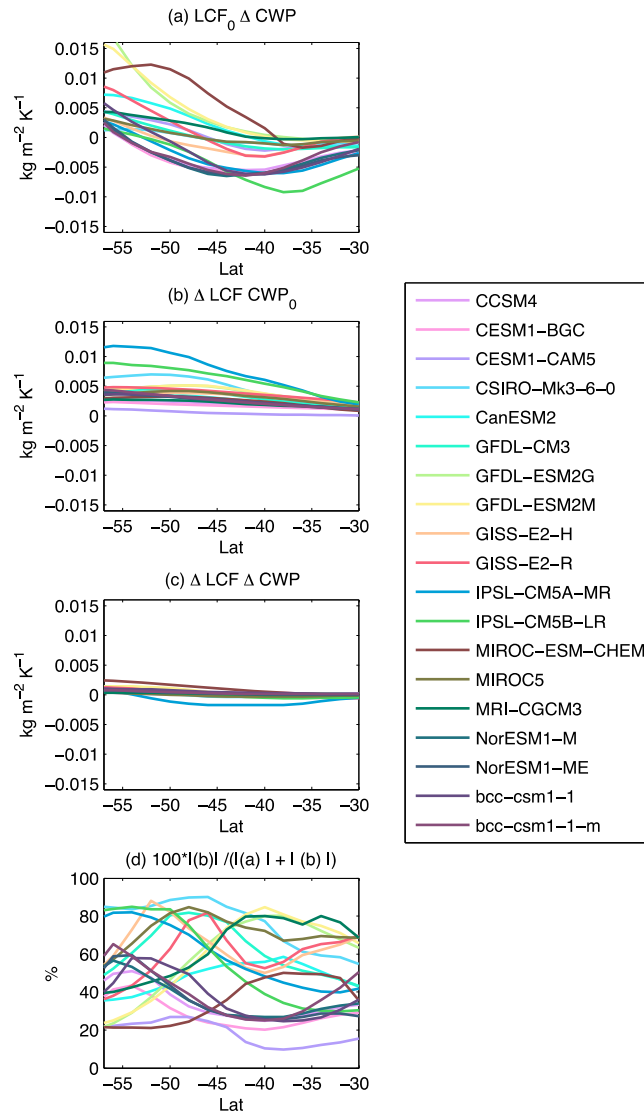


Figure 2. The contributions to (a) changes in LWP from condensate mass changes, (b) changes in partitioning, and (c) the cross term of partitioning and condensate mass changes. (d) The fraction of the magnitude of the condensate and partitioning terms explained by the partitioning term. These terms are described in equation (1). All changes in LWP are normalized by the change in zonal mean air temperature at 850 hPa. Models are listed in the legend.

4. Calculation of Impact Due To Phase Partitioning

Although we cannot easily separate the mechanisms that drive the changing condensate mass in GCMs, we can investigate the impacts of condensate partitioning by representing the change in LWP between historical and warmed climates as a Taylor series. For a given location and month in the climatology from CMIP5 we can write

$$\Delta \text{LWP} = \sum_p [\Delta \text{CWP}(p) \cdot \text{LCF}_0(p) + \Delta \text{LCF}(p) \cdot \text{CWP}_0(p) + \Delta \text{LCF}(p) \cdot \Delta \text{CWP}(p)] \quad (1)$$

where Δ represents a difference between the historical data and warmed data, $\text{CWP}(p)$ is the condensate (ice plus liquid) mass (kg/m^2) integrated through a model pressure level at pressure (p), rather than the entire atmospheric column, LCF is the liquid fraction in a model pressure level defined as $\text{LWP}(p)/(\text{IWP}(p) + \text{LWP}(p))$, and the subscript 0 indicates the historical state. The LCF in GCMs is found to be a smooth function of temperature (Figure 1a), and thus, we approximate LWP as a function of air temperature only, using the curves in Figure 1a.

$$\text{LCF}(\text{LWP}(p), \text{IWP}(p)) \rightarrow \text{LCF}(T(p)) \quad (2)$$

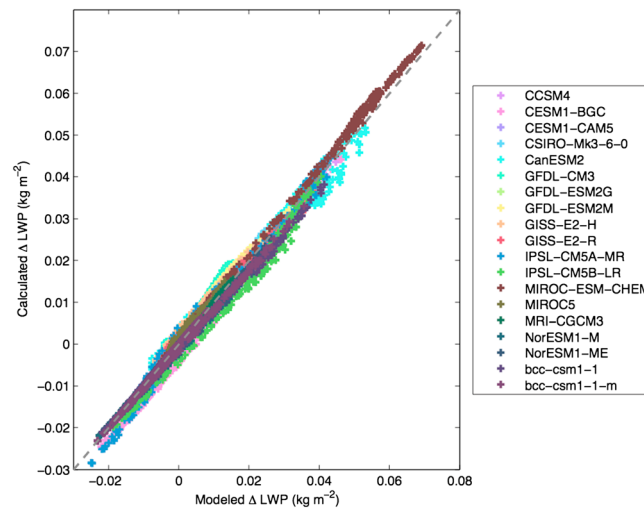


Figure 3. Change in LWP between the historical and RCP8.5 experiments calculated from equation (1) using the curves of liquid over total condensate as a function of temperature from Figure 1 compared to the LWP change predicted by each model. The one-to-one line is shown with grey dashes. The monthly zonal mean change in LWP at each latitude is shown as crosses. Models are listed in the legend.

Calculation of the change in LWP using equation (1) and the curves shown in Figure 1 yields strong agreement with the modeled zonal mean LWP change (Figure 3). This demonstrates that (1) the curves shown in Figure 1 are sufficiently exact to investigate the LWP response in a warmed climate and (2) the LCF dependence on temperature in GCMs is approximately invariant under climate change for the purposes of examining the change in LWP.

In the multimodel mean, about half of the change in LWP can be attributed to repartitioning, but the relative sizes of the condensate and partitioning components vary considerably (Figure 2d). Changes in condensate mass significantly affect the change in LWP (Figure 2a). The condensate mass term increases LWP at higher latitudes and decreases LWP at lower latitudes. The decrease in LWP at lower latitudes is due to a combination of decreases in cloud fraction and, to a lesser degree, optical depth [Zelinka *et al.*, 2012a, 2013]. We will discuss some potential mechanisms that decrease cloud fraction shortly. In contrast to the condensate term, the partitioning term acts to uniformly increase LWP as the atmosphere warms (Figure 2b). The covariance term in equation (1) plays a negligible role (Figure 2c).

Several mechanisms that are not a function of condensate phase may affect the condensate mass. As mentioned earlier, changes in adiabatic water content, which are proportional to the temperature derivative of the moist adiabat, may increase condensate mass in a warming climate [Betts and Harshvardhan, 1987]. LWP decreases slightly at lower latitudes. Several factors have been shown to affect subtropical cloud fraction and are likely to contribute to the decrease in LWP diagnosed in the more equatorward, and liquid cloud-dominated, latitudes shown in Figure 2. These are drying of the free troposphere, a more emissive free troposphere due to greenhouse gases, reduced wind speed, or larger fluxes of water vapor in the boundary layer. Each of these should act to decrease cloud fraction as the climate warms [Blossey *et al.*, 2013; Bretherton and Blossey, 2014; Bretherton *et al.*, 2013; Mitchell *et al.*, 1989; Rieck *et al.*, 2012; Tsushima *et al.*, 2006; Wetherald and Manabe, 1988]. Finally, the cloud coverage, and subsequently condensate mass, may simply increase as atmospheric stability increases [Caldwell *et al.*, 2013; Klein and Hartmann, 1993; Wood and Bretherton, 2006]. Increasing stability is a robust feature across GCMs, although the relationship between cloud fraction and stability varies significantly among models [Caldwell *et al.*, 2013; Qu *et al.*, 2014; Webb *et al.*, 2013].

The differing microphysical properties of ice and liquid likely make the change in total condensate mass a function of the change in the partitioning of condensate phase [Morrison *et al.*, 2011; Solomon *et al.*, 2011]. Because our repartitioning component only includes the effect of the warming-induced phase changes on LWP and not the possible effect of repartitioning on total condensate mass, our estimate of the

The change in LWP is calculated using equation (1) by linearly interpolating the LCF curve of a given GCM from Figure 1a to that GCM's atmospheric temperature in the historical and warmed climates. This gives a CWP and LCF at every latitude, longitude, month of the year, and pressure level for each GCM, and the change in LCF can be easily computed.

We divide liquid water path changes into contributions from: condensate mass changes (represented by the first term in equation (1)); repartitioning of condensate by phase as atmospheric temperature changes (the second term); and the covariance between phase change and condensate mass (the third term). The contributions from each term in equation (1) are shown in Figure 2. The overall LWP response is then calculated using equation (1).

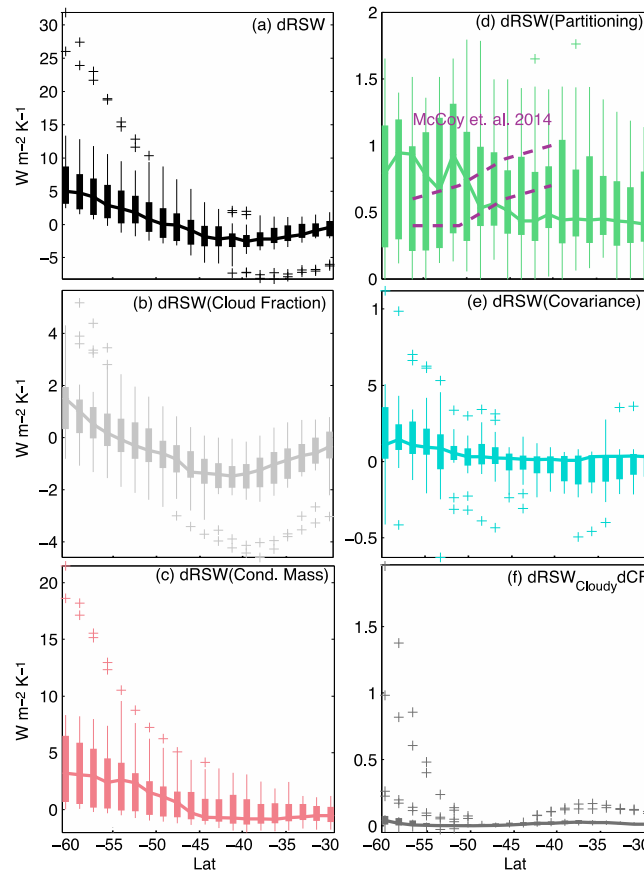


Figure 4. The change in RSW estimated using RRTMG. Changes in LWP, IWP, and CF relative to the historical climate are normalized by change in the zonal mean air temperature at 850 hPa. Calculations are described in the text. The 25th and 75th percentiles of the change in RSW at each latitude are shown as a solid box. Medians are connected using a solid line. Thin lines represent the extrema. Outliers are shown as crosses. (a) The change in all-sky RSW, (b) the change in RSW due to changes in cloud fraction, (c) changes in RSW due to changes in condensate mass, (d) changes in RSW due to repartitioning of condensate, (e) changes in RSW due to the covariance term in equation (1), and (f) the covariance term between changes in cloud fraction and overcast RSW. The observationally estimated range for the partitioning-induced change in RSW from McCoy et al. [2014a] for a fixed liquid effective radius is shown by dashed purple lines in Figure 4d. Note that the y axis range varies among panels.

importance of condensate repartitioning on changes in LWP is likely a lower bound. Model sensitivity studies show that condensate phase is likely to affect condensate mass through differences in the precipitation efficiencies and radiative properties of ice and liquid [Klein et al., 2009; Komurcu et al., 2014; P. Ceppi et al., Mechanisms of the negative shortwave cloud feedback in mid to high latitudes, submitted to *Journal of Climate*, 2015]. Without a detailed investigation of each GCM considered in this study, however, we must assume that the high-latitude LWP response due to the condensate mass term in equation (1) is not a function of the condensate partitioning in a warmed climate. In section 5 we discuss the diagnosed dependence of condensate mass on condensate phase.

It is of interest to estimate the radiative impact of changes in LWP and IWP that are due to the contributions of the condensate mass, partitioning, and covariance terms from equation (1). The intricacies of accurately representing the upwelling SW in the SO have been shown elsewhere [McCoy et al., 2014b]; however, we offer here an approximate calculation to put the individual contributors to changes in LWP in context. This is useful as it includes the effects of the different effective radii of ice and liquid, the nonlinear relationship between optical depth and upwelling SW, and the effects of changes in solar zenith angle throughout the year and with latitude. It should be noted here that our intention is not to reproduce the radiative response of each model but to estimate what their radiative response would be if their microphysics were unified and consistent with observations.

The Rapid Radiative Transfer Model for GCMs (RRTMG) [Mlawer et al., 1997] is used to calculate the upwelling SW at each latitude and month. Clouds are assumed to be homogeneous, and the liquid and ice water paths are uniformly distributed across the coverage assigned by the vertically integrated cloud fraction diagnosed by each model. The cloud is assumed to extend from 800 hPa to 680 hPa. An effective radius of 14 μm is assumed for liquid and 50 μm for ice. These effective radii are consistent with the annual mean values retrieved by, respectively, Moderate Resolution Imaging Spectroradiometer and Cloudsat over the SO [McCoy et al., 2014b].

The change in reflected shortwave (RSW) is calculated using the change in cloud fraction for each model and the change in LWP and IWP calculated from equation (1) (Figure 4). In-cloud IWP (ICIWP) and LWP (ICLWP) are calculated as IWP/CF and LWP/CF. CF is total cloud fraction. It should be noted that the calculation of the change in RSW using monthly data and each model's cloud fraction (as opposed to a simulated satellite cloud

The change in reflected shortwave (RSW) is calculated using the change in cloud fraction for each model and the change in LWP and IWP calculated from equation (1) (Figure 4). In-cloud IWP (ICIWP) and LWP (ICLWP) are calculated as IWP/CF and LWP/CF. CF is total cloud fraction. It should be noted that the calculation of the change in RSW using monthly data and each model's cloud fraction (as opposed to a simulated satellite cloud

fraction) is meant to yield only an approximate change in RSW for the purpose of estimating the impact on RSW of the changes in LWP and IWP predicted by equation (1).

All-sky RSW is written as follows:

$$RSW_{All-sky} = RSW_{Cloudy} \times CF + RSW_{Clear} \times (1 - CF) \quad (3)$$

where the overcast RSW is a function of the in-cloud IWP and LWP

$$RSW_{Cloudy} = RSW_{Cloudy}(ICLWP, ICIWP) \quad (4)$$

CF is the total cloud fraction predicted by the GCM, and RSW_{Clear} is the clear-sky RSW [Cess, 1976]. The change in all-sky RSW between the historical and warmed climates may be written

$$dRSW = RSW_1 - RSW_0 \quad (5)$$

where subscript 1 indicates the warmed climate, and subscript 0 indicates the historical climate. The RSW in each climate state is

$$RSW_1 = RSW_1\left(\frac{LWP_1}{CF_1}, \frac{IWP_1}{CF_1}, RSW_{Clear}\right) \quad (6)$$

$$RSW_0 = RSW_0\left(\frac{LWP_0}{CF_0}, \frac{IWP_0}{CF_0}, RSW_{Clear}\right) \quad (7)$$

where the change in CF, LWP, and IWP relative to the historical climate is divided by the difference in air temperature at 850 hPa between historical and warmed climates, and the clear-sky albedo is assumed to be constant. The change in RSW due to changes in cloud fraction, IWP, and LWP changes is shown in Figure 4a. The multimodel median RSW decreases by $2 \text{ W m}^{-2} \text{ K}^{-1}$ at 40°S and increases by $5 \text{ W m}^{-2} \text{ K}^{-1}$ at 60°S .

To evaluate the contribution to the change in RSW between the historical and warmed climates due to the components in equation (1), we first write the change in RSW as

$$dRSW = [RSW_{Cloudy,0} - RSW_{Clear}] \times dCF + dRSW_{Cloudy} \times CF_0 + dRSW_{Cloudy} \times dCF \quad (8)$$

where the first term corresponds to the change in RSW due to changes in cloud fraction and the second term corresponds to the changes in RSW due to changes in cloud reflectivity. The change in RSW due to the third term involving the product of changes is found to be small (Figure 4f). Equatorward of about 45°S the cloud fraction decreases with warming, contributing to an overall decrease in RSW (Figure 4b). The cloud fraction contributes the majority of the decrease equatorward of 45°S , consistent with more refined estimates of the cloud fraction feedback utilizing radiative kernels [Zelinka *et al.*, 2012a, 2013].

We evaluate how each term in equation (1) affects the RSW when clouds are present. Expanding the cloud albedo term

$$CF_0 \times dRSW_{Cloudy} = CF_0 \times [dRSW_{Cloudy}^{CM} + dRSW_{Cloudy}^{Part} + dRSW_{Cloudy}^{Cov}] \quad (9)$$

where the superscripts on the right side of the equation represent the condensate mass, partitioning, and covariance terms, respectively. The change in RSW due to the condensate mass change from equation (1) is estimated as

$$dRSW_{Cloudy}^{CM} = RSW_{Cloudy}(ICLWP_1^{CM}, ICIWP_1^{CM}) - RSW_{Cloudy}(ICLWP_0, ICIWP_0) \quad (10)$$

the in-cloud ice and liquid water paths are

$$ICLWP_1^{CM} = \left[\sum_p [dCWP(p) \cdot LCF_0(p)] + LWP_0 \right] CF_1^{-1} \quad (11)$$

$$ICIWP_1^{CM} = \left[\sum_p [dCWP(p) \cdot (1 - LCF_0(p))] + IWP_0 \right] CF_1^{-1} \quad (12)$$

The initial in-cloud ice and liquid water paths are

$$ICLWP_0 = LWP_0/CF_0, ICIWP_0 = IWP_0/CF_0 \quad (13)$$

Figure 4c shows the change in RSW due to changes in in-cloud ice and liquid water paths consistent with changes in in-cloud condensate mass, while keeping the partitioning at the historical value.

Next we estimate the change in overcast RSW from repartitioning existing condensate. The change in overcast RSW due to repartitioning is given as

$$dRSW_{\text{Cloudy}}^{\text{part}} = RSW_{\text{Cloudy}}(ICLWP_1^{\text{part}}, ICIWP_1^{\text{part}}) - RSW_{\text{Cloudy}}(ICLWP_0, ICIWP_0) \quad (14)$$

The in-cloud liquid and ice water paths that are created by redistributing the phase of the historical condensate are

$$ICLWP_1^{\text{part}} = \left[\sum_p [CWP_0(p) \cdot dLCF(p)] + LWP_0 \right] \times CF_0^{-1} \quad (15)$$

$$ICIWP_1^{\text{part}} = \left[\sum_p [CWP_0(p) \cdot (1 - dLCF(p))] + IWP_0 \right] \times CF_0^{-1} \quad (16)$$

The change in RSW due to shifting the existing condensate to a more liquid dominated state is shown in Figure 4d. The pronounced increase in RSW that we calculate is due only to the change in effective radius as large ice crystals are replaced by smaller, more reflective liquid droplets.

Finally, the change in RSW due to the covariance term in equation (1) is calculated as

$$dRSW_{\text{Cloudy}}^{\text{Cov}} = RSW_{\text{Cloudy}}(ICLWP_1^{\text{Cov}}, ICIWP_1^{\text{Cov}}) - RSW_{\text{Cloudy}}(ICLWP_0, ICIWP_0) \quad (17)$$

where

$$ICLWP_1^{\text{Cov}} = \left[\sum_p [dCWP(p) \cdot dLCF(p)] + LWP_0 \right] \times CF_0^{-1} \quad (18)$$

$$ICIWP_1^{\text{Cov}} = \left[\sum_p [dCWP(p) \cdot (1 - dLCF(p))] + IWP_0 \right] \times CF_0^{-1} \quad (19)$$

The change in overcast RSW due to the covariance term from equation (1) is small (Figure 4e).

In the multimodel mean, the change in the RSW due to the increase in condensate mass is the largest term (Figure 4c). The GFDL-ESM2M and GFDL-ESM2G models both exhibit very large changes in LWP per degree change in air temperature at 850 hPa (Figure 2), and their estimated high-latitude change in RSW is extremely large. In addition to the very large increase in LWP in these models, the large change in RSW may arise in part from the highly approximate nature of our radiative calculations, which assume homogeneous distribution of LWP.

The RSW increases uniformly at all latitudes as the historical condensate is repartitioned (Figure 4d). At high latitudes the partitioning term contributes less to the increase in RSW than the condensate mass term does, but at lower latitudes they are roughly equivalent. This is consistent with the increase in LWP due to the condensate term being larger than the increase due to repartitioning at higher latitudes as shown in Figure 2.

It is interesting to note that the increase in RSW due to the partitioning term as calculated here is near the partitioning-induced change in RSW estimated from observed seasonal changes in the SO [McCoy *et al.*, 2014a]. The observed estimate of the change in RSW was obtained by calculating the difference in upwelling SW radiation due to repartitioning satellite-observed IWP and LWP consistent with a 1 K seasonal warming. Compared to the observational estimate, the models predict a larger change in RSW at higher latitudes and a smaller change in RSW equatorward of 50°S. The calculation performed here is significantly less precise than the observational estimate, which makes it hard to compare them directly, but it is encouraging that the observational estimate is within a few $\text{W m}^{-2} \text{K}^{-1}$ of the multimodel median estimate.

GCMs differ widely in the way they represent the partitioning of condensate phase, mean state CWP, and mean state CF. It appears that the model mean reflected SW response to phase changes is roughly comparable to the observational estimate, although it appears that the increase in RSW calculated here is generally larger than the observational estimate in the midlatitudes. There is also considerable spread in the range of model-estimated changes in RSW due to repartitioning around the observational estimate (Figure 4d). The estimated change in RSW shown here assumes that the effective radii of ice and liquid do not vary between models. Because optical depth depends on both liquid water path and liquid effective radius, assuming that all GCMs have the same liquid and ice effective radii removes a significant source of intermodel variability in the SW cloud feedback, providing that there are not compensating biases in LWP changes and microphysics

among GCMs. GCMs differ significantly in how they represent cloud microphysics [Bender *et al.*, 2011; Engstrom *et al.*, 2014]. Variations in how models change condensate with warming and how they represent cloud microphysics will both significantly affect the warming-induced change in RSW that they predict in mixed-phase regions [McCoy *et al.*, 2014a]. Again, we must note that this calculation is highly approximate and is provided to give context to the changes in LWP in terms of RSW. A more precise calculation could be performed using in a manner similar to McCoy *et al.* [2014b], but this necessitates histograms of simulated optical depth and height [Bodas-Salcedo *et al.*, 2011] to describe cloud heterogeneity. These are only available in a small subset of models and experiments.

5. Condensate Mass Changes as a Function of Condensate Partitioning

As we have stated previously, condensate partitioning and mass changes are related to each other through the differing microphysical and radiative properties of ice and liquid. In this section we investigate possible relationships between partitioning changes and total condensate changes in CMIP5 models.

Providing that condensate mass and partitioning are related, we would expect changes in mass and the dominance of liquid to be correlated. We examine points in latitude, longitude, pressure, and month that transition from ice-dominated to liquid-dominated clouds between the historical and warmed climatologies. The fractional increase of total condensed water path between historical and warmed climates is shown in Figure 5 as a function of the change in LCF. Only cases where the condensate in a given pressure level, location, and time is mixed phase in both the historical and warmed climate are selected. That is to say, we choose a subset of the climatology where LCF has not saturated between the historical and warmed climates so that we can investigate the ice to liquid transition with warming. In addition, only cases where at least a moderate amount of condensate exists ($CWP(p) > 0.01 \text{ kg m}^{-2}$) were considered. For the sake of clarity, points where the LCF was approximately the same between the historical and warmed climates (LCF increased or decreased by less than 0.005) were omitted from the creation of quantiles of dLCF.

As noted above, condensate mass should increase as LCF increases. To assess this, we plot the change in median condensate mass as a function of changes in condensate partitioning for each model in Figure 5. Because there is no a priori reason to expect this relationship to be linear, we quantify the strength of the relationship using Spearman rank correlations. Eleven models show a significant positive Spearman rank correlation ($p < 0.05$) between median fractional increase in condensate mass and increasing LCF (Figure 5). Considerable spread exists about the median change in condensate mass, and six models show a significant negative correlation. Only two models have no correlation. It is important to keep in mind that we are only examining the correlation between condensate mass increase and deglaciation and confounding variables may create these correlations spuriously. Positive correlations between increases in condensate mass and LCF might occur for reasons other than the phase transition, but which are also dependent on temperature. These were discussed in section 4.

Six models show significant decreasing condensate mass with increasing liquid fraction. A possible explanation for this behavior might be that clouds within that model are more dependent on invigoration from latent heat release as liquid transitions to ice. This is consistent with the warmer glaciation temperatures observed in thick, heavily precipitating frontal clouds in the Northern Hemisphere oceans [Naud *et al.*, 2006].

The change in condensate mass when phase does not change between the historical and warmed climates is shown separately in Figure 5 and is subdivided into high and low LCF cases. When condensate is liquid in both historical and warmed climates its mass tends to decrease with warming. This is consistent with liquid clouds thinning for the reasons that we discussed earlier [Bretherton *et al.*, 2013; Tsushima *et al.*, 2006]. Condensate that is ice in both historical and warmed climates tends to increase its mass, but most models do not have appreciable ice that does not transition, at least partially, to liquid.

As discussed earlier, precipitation suppression is thought to play a significant role in linking phase changes to mass changes. The majority of models that had precipitation data available at the time of writing showed a significant rank correlation between decreasing column precipitation (scaled by total condensate mass in each column) and increasing mean LCF in a column (where LCF in at each level is weighted by the vertically resolved condensate mass) (Figure 6). This supports the suppression of precipitation by deglaciation as a common feature of models and acts as a potential mechanism linking the increase in condensate mass to deglaciation.

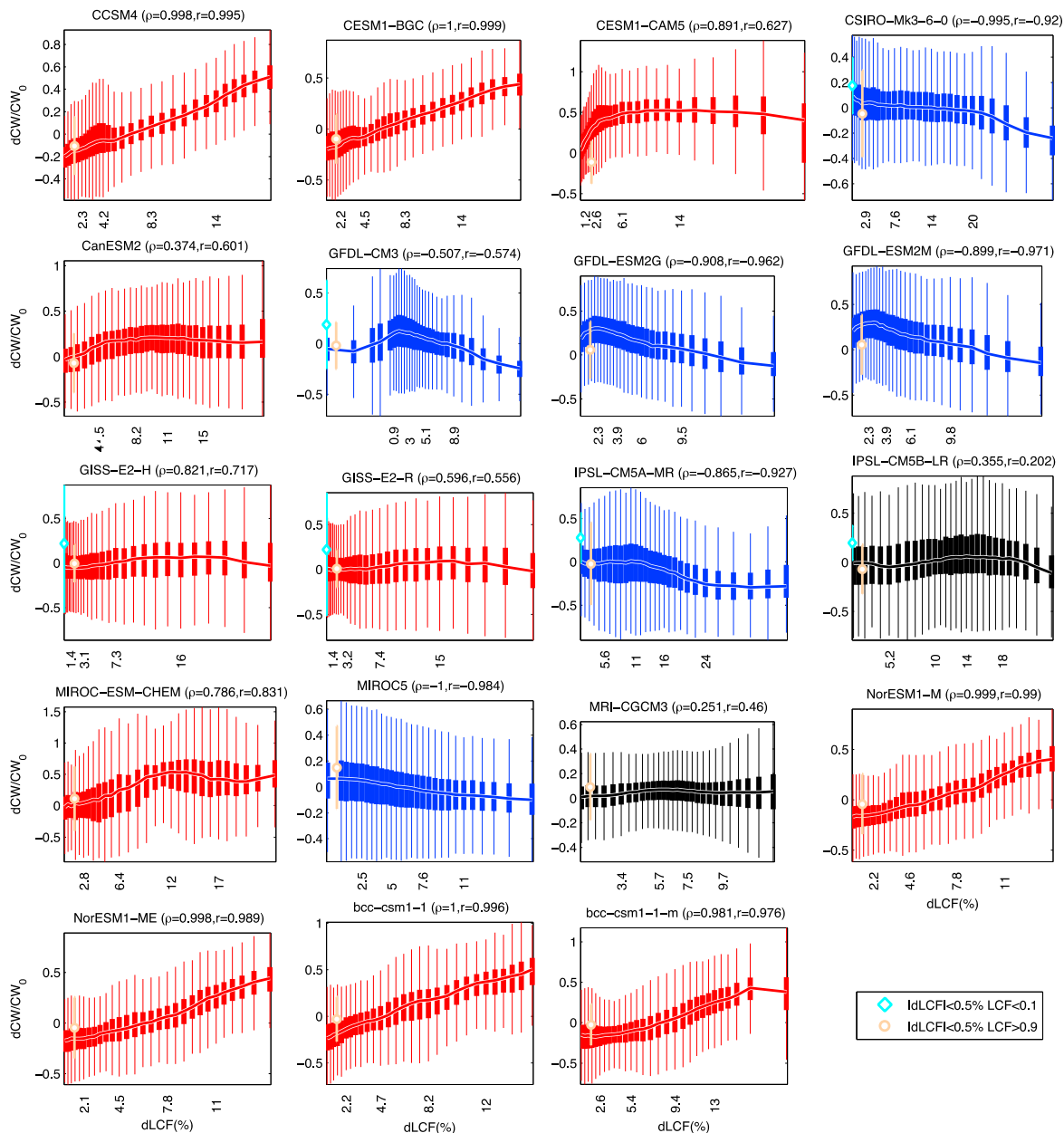


Figure 5. The change in condensate mass binned by change in LCF for each model. The x axis shows change in the fraction of liquid condensate in percent (dLCF \times 100). The y axis shows the change in condensate mass scaled by the historical condensate mass. Bins represent 30 quantiles of the data set. A solid line connects medians. The Spearman rank (ρ) and Pearson linear (r) correlation of the medians are given in the title of each plot. If the rank correlation is significant ($p < 0.05$), then the plots are colored red (positive correlation) or blue (negative correlation). The change in condensate mass when condensate does not change phase by more that 0.5% is shown on the left side of each plot by teal diamonds (LCF $>$ 0.9) and tan circles (LCF $<$ 0.1). If less than 1% of the data set is contained in either of these subsets, that subset is not shown.

While Figure 5 offers a tantalizing glimpse of how the condensate partitioning and cloud schemes in models might interact, disentangling the linkages and mechanisms across GCMs cannot be investigated in the absence of dedicated experimentation within each model. Other insightful studies have shown that cloud phase affects condensate mass in models [Klein et al., 2009; Komurcu et al., 2014; P. Ceppi et al., submitted manuscript, 2015]. The survey of model behavior shown here supports the notion that condensate mass changes are not divorced from condensate phase partitioning, at least in the majority of models investigated here.

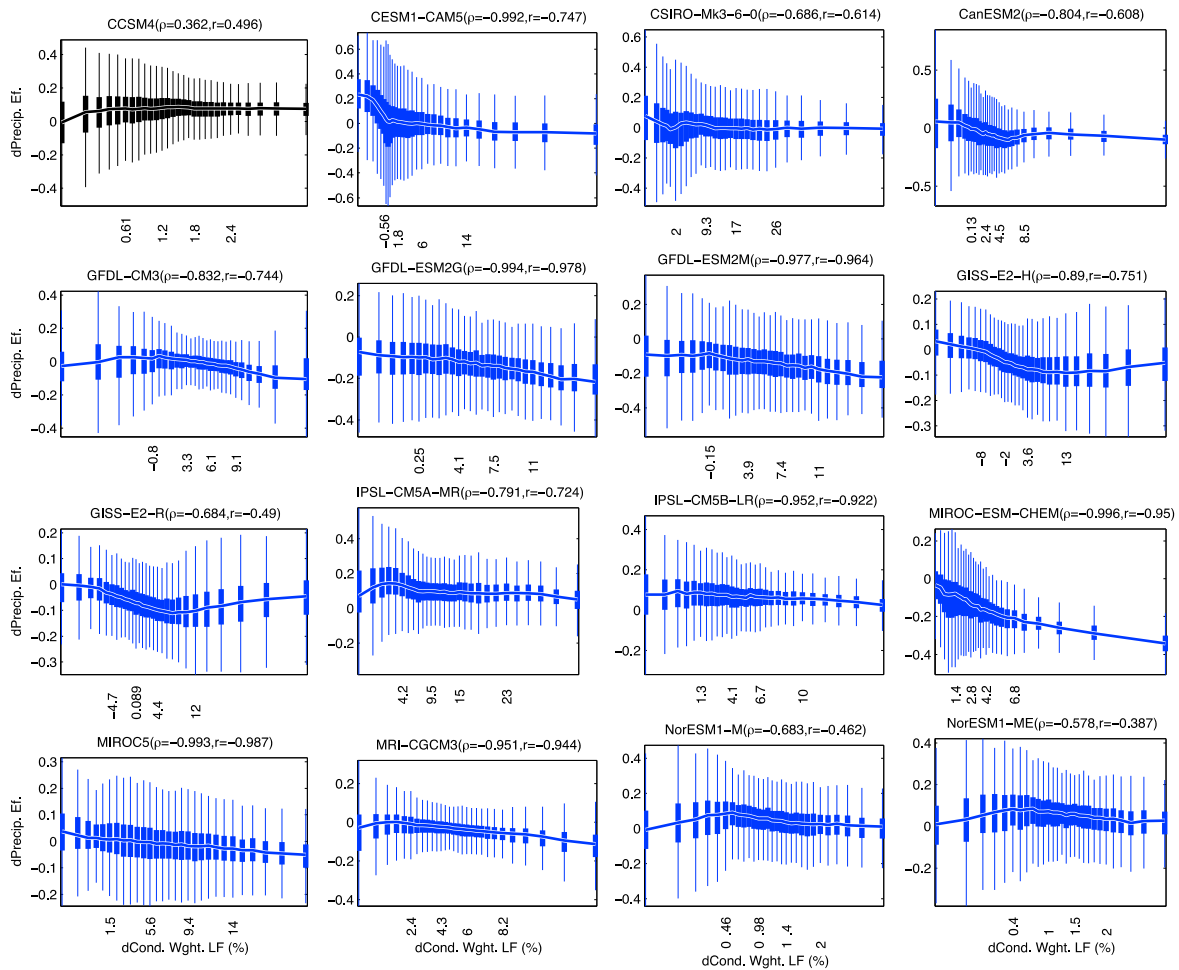


Figure 6. The fractional change in the precipitation efficiency for each GCM as a function of their condensate partitioning in the SO. The y axis shows precipitation efficiency, where precipitation efficiency is defined as the column precipitation divided by the total condensate in the column. The x axis shows the change in the column mean liquid condensate fraction weighted by the condensate mass in each pressure level. Fractional changes are relative to the historical state. The Spearman rank (ρ) and Pearson linear (r) correlation of the medians are given in the title of each plot. At the time of writing three models did not have precipitation fields available for download in the CMIP5 archive and were excluded.

6. The Effects of Variation in Condensate Partitioning

The effective phase partitioning as a function of temperature diagnosed in this study varies significantly across GCMs (Figure 1), and it seems reasonable to assess how much across-model variation in the change in LWP this creates. Even a conservative estimate, as made here, is useful in that it draws attention to the importance of mixed-phase cloud parameterization in GCMs to their high-latitude cloud feedback.

Intermodel variation due to differences in partitioning schemes in the high-latitude LWP change is evaluated by constraining the LCF in equation (1), as opposed to using the native LCF function for each GCM. The atmospheric temperature for each GCM is used in conjunction with the constrained LCF function (described below) to calculate the control and warmed climate LCF. The control and warmed climate LCF may then be used in the three terms of equation (1) in place of each model's native LCF function to calculate the change in LWP. The condensate mass term [$\Delta CWP(p) \cdot LCF_0(T(p))$] is a linear function of control climate LCF. This means that spread in the mass term may be enhanced by the enforcement of a constrained LCF. As we have discussed in section 4, the increase in condensate mass is likely to be a function of the phase partitioning, which is not accounted for by this method. To evaluate the impact of assuming that condensate mass is not a function of phase, we compare the case where the LCF is constrained in all three terms in equation (1) to the case where it is only constrained in the partitioning [$\Delta LCF(T(p)) \cdot CWP_0(p)$] term, while the condensate mass

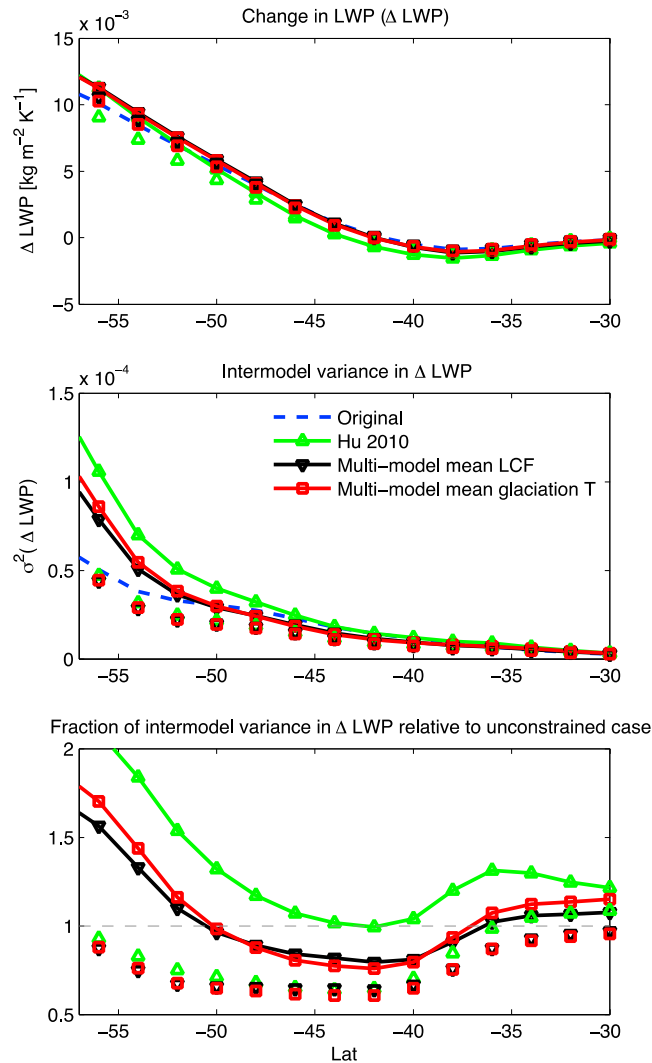


Figure 7. The change in variance in the temperature-normalized change in LWP contingent on the enforcement of a single LCF curve, normalized by change in 850 hPa air temperature. (a) The change in LWP between the historical and warmed climate, (b) the intermodel variance in the predicted change in LWP, and (c) the fractional change in the intermodel variance in the change in LWP. In each figure blue indicates the original model data, red indicates that the glaciation temperatures have been shifted to the multimodel mean, black shows when the multimodel mean LCF curve (Figure 1) has been used instead of each model’s LCF curve, and green shows when the observational LCF from *Hu et al.* [2010] has been used to calculate the change in LWP. If the multimodel mean glaciation temperature or LCF curve has been used to calculate all the terms in equation (1), the symbols are connected by a solid line. If they have only been used to calculate the partitioning term and the condensate mass and covariance terms have been left unchanged, then only symbols are shown.

The variance changes by approximately the same amount if a single glaciation temperature is enforced or if both a single temperature range and glaciation temperature are enforced (Figure 7b). This indicates that the spread in model response with glaciation behavior is primarily due to the spread in glaciation temperature and that the variability in temperature ranges occupied by the mixed-phase regime around the glaciation temperature and distribution of condensate mass as function of temperature in each model do not contribute very strongly to the spread in model response.

and covariance $[\Delta CWP(p) \cdot \Delta LCF(T(p))]$ terms are calculated using the native LCF of each model. We will now discuss the LCF functions that we will use to constrain the LWP response.

We consider three different constraints on the LCF. First, we investigate how much the placement of each models’ LCF curve in terms of temperature affects the spread in LWP changes. Each model’s curve is shifted so that the temperature where $LCF = 0.5$ (the glaciation temperature) is moved to the multimodel mean glaciation temperature, which is 258.4 K, while preserving the shape of the LCF curve. Second, we investigate how much the temperature range that mixed-phase clouds inhabit affects the spread in the change in LWP in the GCMs. The mean LCF curve of all the models (Figure 1) is used to predict the change in LWP. Finally, we enforce the observational LCF curve from *Hu et al.* [2010] and calculate the change in LWP.

The mean LWP change does not vary appreciably upon the enforcement of single glaciation temperature or LCF curve (Figure 7a). When a single glaciation temperature is enforced on all terms in equation (1), decreases in intermodel variance in ΔLWP , normalized by warming, may exceed 20% in the region south of 40°S (Figure 7c). The intermodel variance in ΔLWP increases in the lower latitudes, which are not as persistently mixed phase. However, the intermodel variance in ΔLWP in the regions equatorward of 45°S is relatively small. Thus, the change in intermodel spread in these regions is small in an absolute sense (Figure 7b). The variance also increases in the high latitudes due to spread engendered by the mass term. This is discussed below at more length.

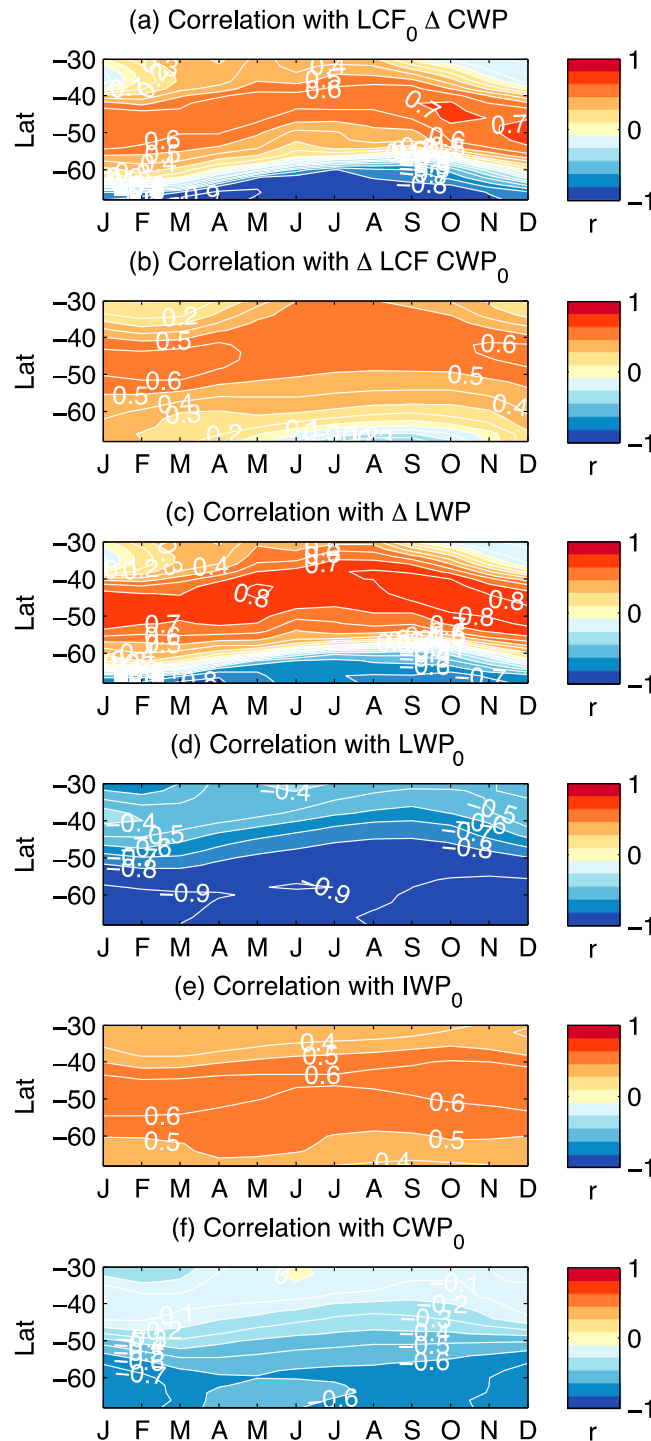


Figure 8. Across-model correlation coefficients (r) as a function of latitude and month between the glaciation temperature and (a) condensate mass change term, (b) condensate partitioning term, (c) total change in LWP, (d) historical LWP, (e) historical IWP, and (f) historical condensed water path. The condensate mass term (Figure 8a), partitioning term (Figure 8b), and overall change in LWP (Figure 8c) are scaled by change in zonal mean air temperature at 850 hPa.

If the multimodel mean LCF or glaciation temperature is enforced for only the partitioning term from equation (1), the variance decreases by up to 40% (Figure 7c). This analysis indicates that the variability engendered by the partitioning term alone is a significant source of intermodel spread.

Finally, the enforcement of the LCF observed by CALIPSO strongly increases the variance in ΔLWP . This is because of the large amount of supercooled liquid in the CALIPSO-detected LCF, which increases the LCF in the control climate in the majority of GCMs (Figure 1) and subsequently increases the spread in the mass term in equation (1). If the LCF from CALIPSO is only enforced on the partitioning term, the decrease in variance is equivalent to the enforcement of the multimodel mean LCF curve or glaciation temperature. Evidently, the relationship between condensate mass and phase remains an important element of constraining the response of LWP to warming. We will now discuss the predictive ability of each models' glaciation temperature alone.

We have shown how the partitioning of ice and liquid in GCMs is dependent on temperature (Figure 1). The repartitioning of ice and liquid as the climate warms contributes significantly to the change in LWP, and it is likely that this repartitioning also affects the overall condensate amount (Figure 5). Given the strong mechanistic linkage we have shown between how a GCM transitions from ice to liquid, it makes sense to ask if the glaciation temperature has some predictive ability regarding the cloud properties in the climate mean state and how they change with warming. The glaciation temperature is correlated with both the mean state and change in LWP across GCMs. Models that glaci-ate at relatively high temperatures (see Figure 1) tend to have a larger increase in LWP and a larger condensate mass change term (Figures 8a and 8c). This is consistent with the idea that a GCM's condensate mass change is, at some level, a function of the condensate phase

change. That is to say, models that have highly glaciated clouds in the mean climate will have a great deal of ice to transition to liquid as the climate warms, and this transition from ice to liquid is also likely to decrease precipitation efficiency. This decrease in precipitation efficiency is consistent with the positive correlation between glaciation temperature and the condensate mass term (Figure 8c). The glaciation temperature is positively correlated across models with climatological IWP and negatively correlated across models with climatological LWP and condensed water path (Figures 8d–8f). Climatological LWP is lower, and IWP is higher in GCMs that more easily nucleate ice, as one would expect. Total condensed water path is generally lower in models that nucleate ice more readily (Figure 8f). This behavior is consistent with precipitation being suppressed in models that create ice at lower temperatures (see sections 1 and 5 for a discussion of precipitation suppression). Significant correlation between model glaciation temperature and the change in midlatitude cloud properties, as shown here, reinforces the importance of a realistic depiction of glaciation in GCMs in order to realistically simulate the midlatitude cloud feedback. The glaciation temperature is also likely to affect model climate sensitivity, since models with warm glaciation temperatures will have more ice at lower latitudes where its transition to liquid can have a greater on reflected shortwave.

7. Summary and Conclusions

Low cloud feedback remains an important source of uncertainty for the sensitivity of Earth's climate. The high-latitude low cloud feedback, which is mainly due to increases in cloud optical depth, is robustly negative, but its magnitude is uncertain. In this study we describe the mechanisms that drive this feedback. Our key points are as follows:

1. GCMs partition condensate in such a way that condensate phase is effectively dependent on temperature on a monthly time scale, but the dependence varies greatly from model to model (Figure 1).
2. The diagnosed partitioning curve represents the GCM behavior well. It may be used to predict the change in LWP due to repartitioning of ice and liquid as the climate warms, taking only the condensate mass and change in atmospheric temperature as input (Figure 3).
3. Between 20% and 80% of the LWP response to warming is due to the repartitioning of condensate as the atmosphere warms (Figure 2d). The intermodel variance in the LWP response is reduced by as much as 20% in the Southern Ocean high latitudes in regions of persistent mixed phase cloud if all models are forced to have the same liquid-ice partitioning dependence on temperature (Figure 7). This represents a minimum contribution from phase changes to the spread in LWP response because differences in the radiative and microphysical characteristics of ice and liquid are likely to link total condensate mass and condensate partitioning (Figure 5) [Klein et al., 2009; McCoy et al., 2014a; Morrison et al., 2011; P. Ceppi et al., Hartmann, and Webb, submitted manuscript, 2015].
4. The temperature at which ice and liquid are equally mixed in a GCM has significant influence on both the mean state and changes in midlatitude clouds. Models that have a warmer glaciation temperature are found to have a larger change in LWP, a lower historical LWP, a higher historical IWP, and a lower historical condensed water path (Figure 8).

Overall, the effect of intermodel differences in climatological ice-liquid condensate partitioning has been shown to strongly contribute to the uncertainty in how clouds change at high latitudes as the climate warms.

References

- Atkinson, J. D., B. J. Murray, M. T. Woodhouse, T. F. Whale, K. J. Baustian, K. S. Carslaw, S. Dobbie, D. O'Sullivan, and T. L. Malkin (2013), The importance of feldspar for ice nucleation by mineral dust in mixed-phase clouds, *Nature*, *498*(7454), 355–358.
- Bender, F. A. M., R. J. Charlson, A. M. L. Ekman, and L. V. Leahy (2011), Quantification of monthly mean regional-scale albedo of marine stratiform clouds in satellite observations and GCMs, *J. Appl. Meteorol. Climatol.*, *50*(10), 2139–2148.
- Betts, A. K., and Harshvardhan (1987), Thermodynamic constraint on the cloud liquid water feedback in climate models, *J. Geophys. Res.*, *92*(D7), 8483–8485, doi:10.1029/JD092iD07p08483.
- Blossey, P. N., C. S. Bretherton, M. H. Zhang, A. N. Cheng, S. Endo, T. Heus, Y. G. Liu, A. P. Lock, S. R. de Roode, and K. M. Xu (2013), Marine low cloud sensitivity to an idealized climate change: The CGILS LES intercomparison, *J. Adv. Model. Earth Syst.*, *5*, 234–258, doi:10.1002/jame.20025.
- Bodas-Salcedo, A., et al. (2011), COSP: Satellite simulation software for model assessment, *Bull. Am. Meteorol. Soc.*, *92*(8), 1023–1043.
- Bony, S., et al. (2006), How well do we understand and evaluate climate change feedback processes?, *J. Clim.*, *19*(15), 3445–3482.
- Bower, K. N., S. J. Moss, D. W. Johnson, T. W. Choullarton, J. Latham, P. R. A. Brown, A. M. Blyth, and J. Cardwell (1996), A parametrization of the ice water content observed in frontal and convective clouds, *Q. J. R. Meteorol. Soc.*, *122*(536), 1815–1844.
- Bretherton, C. S., and P. N. Blossey (2014), Low cloud reduction in a greenhouse-warmed climate: Results from Lagrangian LES of a subtropical marine cloudiness transition, *J. Adv. Model. Earth Syst.*, *6*, 91–114, doi:10.1002/2013MS000250.

Acknowledgments

We acknowledge the World Climate Research Programme's Working Group on Coupled Modelling, which is responsible for CMIP, and we thank the climate modeling centers for producing and making available their model output. For CMIP the U.S. Department of Energy's Program for Climate Model Diagnosis and Intercomparison provides coordinating support and led development of software infrastructure in partnership with the Global Organization for Earth System Science Portals. CMIP5 model data may be downloaded from <http://pcmdi9.llnl.gov>. D.T. McCoy, D.L. Hartmann, and M.D. Zelinka were supported under DOE grant DE-SC0012580, and D.T. McCoy acknowledges government support awarded by DoD, Air Force Office of Scientific Research, National Defense Science and Engineering Graduate (NDSEG) Fellowship, 32 CFR 168a. The effort of M.D. Zelinka was performed under the auspices of the U.S. Department of Energy by Lawrence Livermore National Laboratory under contract DE-AC52-07NA27344. The authors would like to thank Muge Komurcu, Trude Storelvmo, Ivy Tan, Rob Wood, and the three anonymous reviewers for their interesting discussion and advice.

- Bretherton, C. S., P. N. Blossy, and C. R. Jones (2013), Mechanisms of marine low cloud sensitivity to idealized climate perturbations: A single-LES exploration extending the CGILS cases, *J. Adv. Model. Earth Syst.*, *5*, 316–337, doi:10.1002/jame.20019.
- Caldwell, P. M., Y. Y. Zhang, and S. A. Klein (2013), CMIP3 subtropical stratocumulus cloud feedback interpreted through a mixed-layer model, *J. Clim.*, *26*(5), 1607–1625.
- Ceppi, P., M. D. Zelinka, and D. L. Hartmann (2014), The response of the Southern Hemispheric eddy-driven jet to future changes in shortwave radiation in CMIP5, *Geophys. Res. Lett.*, *41*, 3244–3250, doi:10.1002/2014GL060043.
- Cesana, G., D. E. Waliser, X. Jiang, and J. L. F. Li (2015), Multi-model evaluation of cloud phase transition using satellite and reanalysis data, *J. Geophys. Res. Atmos.*, doi:10.1002/2014JD022932.
- Cess, R. D. (1976), Climate change: An appraisal of atmospheric feedback mechanisms employing zonal climatology, *J. Atmos. Sci.*, *33*(10), 1831–1843.
- Cheng, A. N., K. M. Xu, Y. X. Hu, and S. Kato (2012), Impact of a cloud thermodynamic phase parameterization based on CALIPSO observations on climate simulation, *J. Geophys. Res.*, *117*, D09103, doi:10.1029/2011JD017263.
- Choi, Y. S., C. H. Ho, C. E. Park, T. Storelvmo, and I. Tan (2014), Influence of cloud phase composition on climate feedbacks, *J. Geophys. Res. Atmos.*, *119*, 3687–3700, doi:10.1002/2013JD020582.
- Chubb, T. H., J. B. Jensen, S. T. Siems, and M. J. Manton (2013), In situ observations of supercooled liquid clouds over the Southern Ocean during the HIAPER Pole-to-Pole Observation campaigns, *Geophys. Res. Lett.*, *40*, 5280–5285, doi:10.1002/grl.50986.
- Engstrom, A., F. A. M. Bender, and J. Karlsson (2014), Improved representation of marine stratocumulus cloud shortwave radiative properties in the CMIP5 climate models, *J. Clim.*, *27*(16), 6175–6188.
- Frierson, D. M. W., and Y. T. Hwang (2012), Extratropical influence on ITCZ shifts in slab ocean simulations of global warming, *J. Clim.*, *25*(2), 720–733.
- Grosvenor, D. P., T. W. Choulaton, T. Lachlan-Cope, M. W. Gallagher, J. Crosier, K. N. Bower, R. S. Ladkin, and J. R. Dorsey (2012), In-situ aircraft observations of ice concentrations within clouds over the Antarctic Peninsula and Larsen Ice Shelf, *Atmos. Chem. Phys.*, *12*(23), 11,275–11,294.
- Hu, Y. X., et al. (2009), CALIPSO/CALIOP cloud phase discrimination algorithm, *J. Atmos. Oceanic Technol.*, *26*(11), 2293–2309.
- Hu, Y. X., S. Rodier, K. M. Xu, W. B. Sun, J. P. Huang, B. Lin, P. W. Zhai, and D. Josset (2010), Occurrence, liquid water content, and fraction of supercooled water clouds from combined CALIOP/IIR/MODIS measurements, *J. Geophys. Res.*, *115*, D00H34, doi:10.1029/2009JD012384.
- Huang, Y., S. T. Siems, M. J. Manton, A. Protat, and J. Delanoe (2012), A study on the low-altitude clouds over the Southern Ocean using the DARDAR-MASK, *J. Geophys. Res.*, *117*, D18204, doi:10.1029/2012JD017800.
- Kanitz, T., P. Seifert, A. Ansmann, R. Engelmann, D. Althausen, C. Casaccia, and E. G. Rohwer (2011), Contrasting the impact of aerosols at northern and southern midlatitudes on heterogeneous ice formation, *Geophys. Res. Lett.*, *38*, L17802, doi:10.1029/2011GL048532.
- Klein, S. A., and D. L. Hartmann (1993), The seasonal cycle of low stratiform clouds, *J. Clim.*, *6*(8), 1587–1606.
- Klein, S. A., et al. (2009), Intercomparison of model simulations of mixed-phase clouds observed during the ARM Mixed-Phase Arctic Cloud Experiment. I: Single-layer cloud, *Q. J. R. Meteorol. Soc.*, *135*(641), 979–1002.
- Komurcu, M., T. Storelvmo, I. Tan, U. Lohmann, Y. X. Yun, J. E. Penner, Y. Wang, X. H. Liu, and T. Takemura (2014), Intercomparison of the cloud water phase among global climate models, *J. Geophys. Res. Atmos.*, *119*, 3372–3400, doi:10.1002/2013JD021119.
- McCoy, D. T., D. L. Hartmann, and D. P. Grosvenor (2014a), Observed Southern Ocean cloud properties and shortwave reflection. Part II: Phase changes and low cloud feedback, *J. Clim.*, *27*(23), 8858–8868.
- McCoy, D. T., D. L. Hartmann, and D. P. Grosvenor (2014b), Observed Southern Ocean cloud properties and shortwave reflection. Part I: Calculation of SW flux from observed cloud properties, *J. Clim.*, *27*(23), 8836–8857.
- Mitchell, J. F. B., C. A. Senior, and W. J. Ingram (1989), CO₂ and climate—A missing feedback, *Nature*, *341*(6238), 132–134.
- Mlawer, E. J., S. J. Taubman, P. D. Brown, M. J. Iacono, and S. A. Clough (1997), Radiative transfer for inhomogeneous atmospheres: RRTM, a validated correlated-k model for the longwave, *J. Geophys. Res.*, *102*(D14), 16,663–16,682, doi:10.1029/97JD00237.
- Morrison, H., G. de Boer, G. Feingold, J. Harrington, M. D. Shupe, and K. Sulia (2011), Resilience of persistent Arctic mixed-phase clouds, *Nat. Geosci.*, *5*(1), 11–17.
- Murray, B. J., D. O'Sullivan, J. D. Atkinson, and M. E. Webb (2012), Ice nucleation by particles immersed in supercooled cloud droplets, *Chem. Soc. Rev.*, *41*(19), 6519–6554.
- Naud, C. M., A. D. Del Genio, and M. Bauer (2006), Observational constraints on the cloud thermodynamic phase in midlatitude storms, *J. Clim.*, *19*(20), 5273–5288.
- Naud, C. M., A. D. Del Genio, M. Haefelin, Y. Morille, V. Noel, J. C. Dupont, D. D. Turner, C. Lo, and J. Comstock (2010), Thermodynamic phase profiles of optically thin midlatitude clouds and their relation to temperature, *J. Geophys. Res.*, *115*, D11202, doi:10.1029/2009JD012889.
- Qu, X., A. Hall, S. Klein, and P. Caldwell (2014), On the spread of changes in marine low cloud cover in climate model simulations of the 21st century, *Clim. Dyn.*, *42*(9–10), 2603–2626.
- Rauber, R. M., and A. Tokay (1991), An explanation for the existence of supercooled water at the top of cold clouds, *J. Atmos. Sci.*, *48*(8), 1005–1023.
- Rieck, M., L. Nuijens, and B. Stevens (2012), Marine boundary layer cloud feedbacks in a constant relative humidity atmosphere, *J. Atmos. Sci.*, *69*(8), 2538–2550.
- Solomon, A., M. D. Shupe, P. O. G. Persson, and H. Morrison (2011), Moisture and dynamical interactions maintaining decoupled Arctic mixed-phase stratocumulus in the presence of a humidity inversion, *Atmos. Chem. Phys.*, *11*(19), 10,127–10,148.
- Tan, I., T. Storelvmo, and Y.-S. Choi (2014), Spaceborne lidar observations of the ice-nucleating potential of dust, polluted dust, and smoke aerosols in mixed-phase clouds, *J. Geophys. Res. Atmos.*, *119*, 6653–6665, doi:10.1002/2013JD021333.
- Tsushima, Y., S. Emori, T. Ogura, M. Kimoto, M. J. Webb, K. D. Williams, M. A. Ringer, B. J. Soden, B. Li, and N. Andronova (2006), Importance of the mixed-phase cloud distribution in the control climate for assessing the response of clouds to carbon dioxide increase: A multi-model study, *Clim. Dyn.*, *27*(2–3), 113–126.
- Vial, J., J. L. Dufresne, and S. Bony (2013), On the interpretation of inter-model spread in CMIP5 climate sensitivity estimates, *Clim. Dyn.*, *41*(11–12), 3339–3362.
- Webb, M. J., F. Lambert, and J. M. Gregory (2013), Origins of differences in climate sensitivity, forcing and feedback in climate models, *Clim. Dyn.*, *40*(3–4), 677–707.
- Wetherald, R. T., and S. Manabe (1988), Cloud feedback processes in a general-circulation model, *J. Atmos. Sci.*, *45*(8), 1397–1415.
- Wood, R., and C. S. Bretherton (2006), On the relationship between stratiform low cloud cover and lower-tropospheric stability, *J. Clim.*, *19*(24), 6425–6432.

- Zelinka, M. D., S. A. Klein, and D. L. Hartmann (2012a), Computing and partitioning cloud feedbacks using cloud property histograms. Part II: Attribution to changes in cloud amount, altitude, and optical depth, *J. Clim.*, *25*(11), 3736–3754.
- Zelinka, M. D., S. A. Klein, and D. L. Hartmann (2012b), Computing and partitioning cloud feedbacks using cloud property histograms. Part I: Cloud radiative kernels, *J. Clim.*, *25*(11), 3715–3735.
- Zelinka, M. D., S. A. Klein, K. E. Taylor, T. Andrews, M. J. Webb, J. M. Gregory, and P. M. Forster (2013), Contributions of different cloud types to feedbacks and rapid adjustments in CMIP5*, *J. Clim.*, *26*(14), 5007–5027.